ORIGINAL ARTICLE

Design of Lattice Structures Using Local Relative Density Mapping Method

Guo-Hua Song[1], Shi-Kai Jing[2*], Fang-Lei Zhao[2], Ye-Dong Wang[2], Hao Xing[2] and Long-Fei Qie[2]

Abstract

In order to solve the problem of substantial computational resources of lattice structure during optimization, a local relative density mapping (LRDM) method is proposed. The proposed method uses solid isotropic microstructures with penalization to optimize a model at the macroscopic scale. The local relative density information is obtained from the topology optimization result. The contour lines of an optimized model are extracted using a density contour approach, and the triangular mesh is generated using a mesh generator. A local mapping relationship between the elements' relative density and the struts' relative cross-sectional area is established to automatically determine the diameter of each individual strut in the lattice structures. The proposed LRDM method can be applied to local finite element meshes and local density elements, but it is also suitable for global ones. In addition, some cases are considered in order to test the effectiveness of the LRDM method. The results show that the solution time of the LRDM is lower than the RDM method by approximately 50%. The proposed method provides instructions for the design of more complex lattice structures.

Keywords: Lattice structures, Local relative density mapping, Topology optimization, Additive manufacturing

1 Introduction

Additive manufacturing (AM), also known as 3D printing, refers to a process by which a 3D digital model is used to build a part or product by depositing material in layers. The advantage of AM is that it can provide designers with great opportunities to maximize the performance of their designed products through the synthesis of shapes, sizes, hierarchical structures, and material composition [1]. To an extent, AM can not only reduce material costs but also speed up novel and/or conceptual designs, especially with the use of foam, honeycomb structures, and lattice structures. The area of lattice structures has received considerable attention owing to their excellent properties: they can be designed and used for multiple purposes, such as weight reduction, heat transfer, energy absorption, thermal and protection [2–6]. The lattice structure with a relative density of 10% is approximately three times stronger than foam [1].

However, it is a challenging task to design lattice structures owing to their geometric complexities and prohibitive computational costs in the design process. In the past few decades, several approaches were put forward for the design of lattice structures or mesoscale truss structures with a strut diameter in the range of 0.1 mm to 10 mm, and these methods can be roughly classified into two categories: solid modeling techniques and optimization techniques.

Wang and Rosen developed a computer-aided design tool for designing truss structures that could easily be incorporated into 3D printed parts [7]. Wallach et al. [8] designed a 3D periodic truss structure using the linear array command. They analyzed the elastic moduli as well as the uniaxial and shear strengths of the truss structures. Wang et al. [9] proposed a parametric modeling method for truss-like structures. Based on a unit cell approach, a conformal lattice structure is designed to enhance the performance of the cellular structure that was developed by Wang [10]. For large truss-like cellular structures, computational complexities can cause difficulties in CAD modeling, and therefore, Wang et al. [11] introduced a hybrid geometric modeling method. From the

*Correspondence: jingshikai@bit.edu.cn
[2] School of Mechanical Engineering, Beijing Institute of Technology, Beijing 100081, China
Full list of author information is available at the end of the article

Song *et al. Chin. J. Mech. Eng.*   (2018) 31:89

Page 2 of 9

above analysis, we can see that solid modeling methods are primarily used for generating truss/lattice structures without considering the optimization problem. Moreover, optimization techniques can also be an effective tool for designing truss/lattice structures. Typical optimization approaches, such as the ground truss approach and homogenization method, synthesize the topology and geometry of the truss structures [12, 13]. Chu et al. [14] presented a synthesis method using particle swarm optimization and least-squares minimization for designing components comprised of cellular structures. The optimization approaches of truss structures are limited by the computational demands of a great number of design variables and/or by the memory limitations of computers [15–18].

Therefore, one of the key problems is how to optimize lattice structures such that the potential for mass reduction and computational costs can be fully realized in the design process. A non-iterative size, matching, and scaling (SMS) method was proposed by Graf et al. [19]. It eliminates the need for time-consuming optimization by using a combination of a solid-body finite element analysis and a pre-defined lattice configuration to generate a structure's lattice topology. However, the non-iterative SMS approach lacked a truly systematic methodology [20]. To counter the traditional manufacturing limitation, Chang et al. [21] presented a new SMS method in order to take advantage of the potential of additive manufacturing. To address the drawbacks of the SMS approach in determining the appropriate diameters for the structure's struts, a new augmented SMS method that incorporates conformal lattice structure construction methods was presented by Nguyen et al. [22]. They studied the process of generation of lattice structures for a complex shape. However, the design of lattice structures using various SMS methods is only applicable in the case of targeted loading. These methods cannot be used in the case of multiple loading conditions. In addition, a relative density mapping (RDM) method was developed to obtain lattice structures that are capable of handling multi-loading conditions without additional computational costs [23]. However, there exist some problems with the principles of the RDM method. Firstly, one of assumptions made is that the relative cross-section diameter of each strut is dependent on the contribution of all the relevant density elements. The distance calculation requires much computational resources due to its exponential time complexity. Moreover, the relative density elements include several 0 values, which do not contribution for the strut. Furthermore, the RDM method does not guarantee the structural strength of the generated lattice structures during the mapping process.

To further reduce the computational costs and to improve the performance of the lattice structures,an LRDM method is presented. First, the SIMP method is used to gain a topology optimization result at the macroscopic scale. The relative density contour is then extracted using the density contour approach and a triangular mesh is generated using a mesh generation algorithm. Finally, a new mapping relationship between the local relative densities and local finite element mesh (FEM) is established to generate the lattice structures. The rest of this paper is organized as follows. We first describe a mesh generating process in Section 2. In Section 3, we present the LRDM method, and in Section 4, some case studies are used to verify the effectiveness and efficiency of the proposed method. The conclusions drawn are presented in the final section.

2 Mesh Generating Process

The LRDM method uses the triangular FEM because it is difficult to approximate the part's surface for the unit-cell type mesh used in the RDM method. In order to generate the mesh configuration in the optimized region of the topology optimization result, three following steps are required to be taken.

2.1 Generating Relative Density Point Cloud

First, a density threshold value is set to obtain the point cloud data. The cloud point is set as 1 where the relative density is greater than or equal to the threshold value else, it is set as 0. The formula for the could points is given in Eq. (1). In addition, in order to ensure that the sum of the relative density values remains unchanged, the total number of grayscale elements must be a constant during their conversion to cloud points.

$$g(x,y) = \begin{cases} 255, & \text{if } f(x,y) \geq T, \\ 0, & \text{otherwise,} \end{cases} \tag{1}$$

where $f(x,y)$ is the set of the relative density, and $g(x,y)$ is the set of cloud points. The sum of $f(x,y)$ and $g(x,y)$ must be zero. The suitable density threshold value T can then be determined by using the bisection algorithm.

$$\Delta V = \sum f(x,y) - \sum g(x,y). \tag{2}$$

2.2 Density Contour Approach

Although there is no intermediate relative density value in the point cloud data obtained from step (1), there is still a jagged border. In order to obtain a smooth boundary, a density contour method is used to reassign the relative density of each element to each node point, and the density contour is obtained using the interpolation

Song *et al. Chin. J. Mech. Eng.* (2018) 31:89

Page 3 of 9

approach. The relative density of the nodes can be calculated by using an average weight function, and the interpolation formula is given in Eq. (3). The contour line was reconstructed using the density contour approach and B-spline curves [24]:

$$\rho_k = \frac{1}{M} \sum_{i=1}^{M} \rho_{k,i}, \qquad (3)$$

where ρ_k is the relative density of the kth node, M is the number of neighboring elements at this node, and $\rho_{k,i}$ is the relative density of the ith neighboring element of the kth node.

2.3 Triangular Mesh Generation
After obtaining the relative density contour from step (2), the triangular mesh is generated using a mesh generation algorithm [25, 26]. The Delaunay algorithm cannot generate a high-quality triangular mesh as there is no cloud data inside the boundary contours. Thus, in order to generate a high-quality triangular mesh, the following steps are required to be followed. First, the Delaunay algorithm is implemented to generate the initial triangular mesh. The mesh can then be optimized and adjusted locally using the mesh generation [26, 27]. The advantage of this approach is that it does not generate an elongated triangular mesh. The mesh generation process is illustrated in Figure 1.
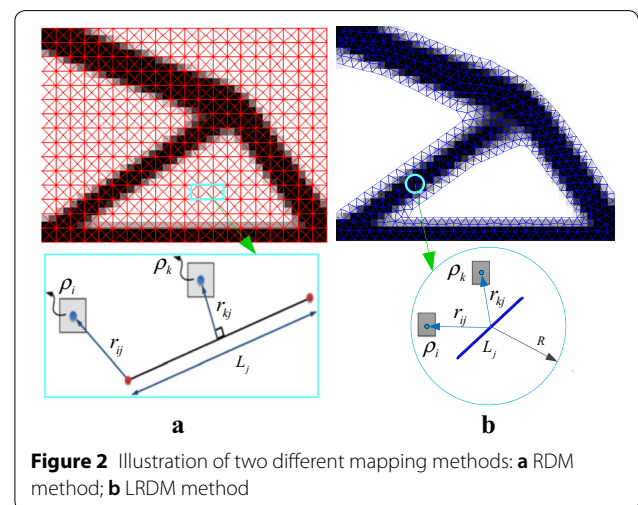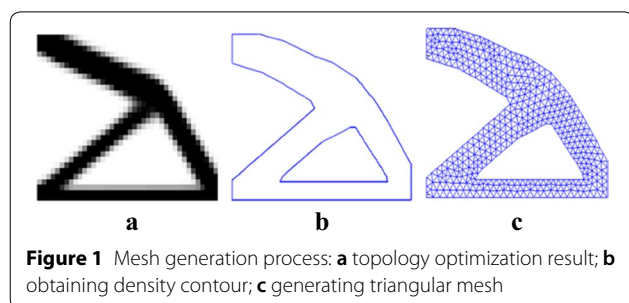
3 LRDM Method
3.1 Formulation of LRDM Method
The computational cost can be further reduced by using our proposed schemes. Firstly, it seems reasonable to assume that the relative cross-section diameter of the strut must depend on the local relative densities. The local relative densities refer to the density elements that are located in the range of a circle of radius R having its center at the midpoint of the strut. Secondly, it is possible to reduce the number of FEM by using the mesh generation process in Section 2. Thirdly, an improved strategy

of the distance weight function is presented to reduce the calculation time. The conditions assumed for the RDM and LRDM methods are shown in Figure 2a, b respectively. RDM uses the relative densities of the topology optimization and global FEM mesh. LRDM uses local relative densities having a non-zero value and the local FEM mesh. The local FEM mesh refers to the mesh that is located in the optimized region of the topology optimization result.

The key process in the RDM method is the calculation of the distance of all the relative density elements from each line segment in the FEM mesh. The RDM method requires a substantial amount of computing resources because of its exponential time complexity. Moreover, it implements three judgement conditions for determining which relative density element is at the shortest distance from the two endpoints or pedals of each line segment, as shown in Figure 2a. The algorithm efficiency is low for a unit-cell of a few millimeters. To alleviate these deficiencies, three steps can be taken to improve the efficiency of the RDM algorithm. First, the local relative densities are used to replace the global ones. Secondly, we can reduce the number of meshes with a local mesh in the optimized region. Thirdly, a new distance formula is derived for the LRDM method. Let us assume that there are m relative density elements within the range of the circle j (as shown in Figure 2b), and thus, the improved formula for mapping the relative density of m elements to the struts is given in Eq. (4):

$$Ar_j = \frac{\sum_{i=1}^{m} \rho_i \omega(r_{ij})}{m}, \qquad (4)$$

Figure 1 Mesh generation process: **a** topology optimization result; **b** obtaining density contour; **c** generating triangular mesh

Figure 2 Illustration of two different mapping methods: **a** RDM method; **b** LRDM method

Song *et al. Chin. J. Mech. Eng.* (2018) 31:89

Page 4 of 9

where Ar_j is the relative cross-sectional area of the strut, ρ_i is the relative density, ω is a weight function, m is the number of elements within the radius R, and r_{ij} is the distance of element i from strut j. The advantage of the new formula is that it can reduce the computational costs incurred by reducing the number of relative density elements that are far away from the strut during the mapping process. In addition, a general weight function is also proposed, and its formula is given in Eq. (5):

$$\omega(r_{ij}) = \exp(-kr_{ij}). \tag{5}$$

To ensure the strut diameter is neither too large nor too small, a lower value $\min(\boldsymbol{Ar})$ and a higher value $\max(\boldsymbol{Ar}) = 1$ for the relative cross-sectional area are set during the mapping process. Therefore, the scaling and adjustment of the strut can be performed according to [23]:

$$Ar_j = \left[\frac{1 - \min(\boldsymbol{Ar})}{\max(\boldsymbol{Ar}) - \min(\boldsymbol{Ar})} \right] \times [Ar_j - \max(\boldsymbol{Ar})] + 1. \tag{6}$$

The next step is to calculate the scaling factor between the relative cross-sectional area and actual cross-sectional area of each strut for the lattice structures. However, it does not guarantee the structure strength of the generated lattice structures because the RDM method uses a fixed volume constraint. Moreover, the strength of lattice structures is governed by their relative density. Therefore, the appropriate relative density may be required to ensure that the elastic modulus of the generated lattice structure is equivalent to the corresponding elastic constants of the topology optimization. According to the Gibson–Ashby model [28], the elastic modulus has a polynomial law relationships with the relative density. For example, for a plane stress problem, the anisotropic constitutive law is $\sigma = \boldsymbol{C}\varepsilon$. A scaling law between relative density and elastic matrix of lattice structures can be written as follows:

$$\boldsymbol{C}(\rho) = \boldsymbol{C}_0 + \boldsymbol{C}_1\rho + \boldsymbol{C}_2\rho^2 + \cdots, \tag{7}$$

where $\boldsymbol{C}$ ($i = 0, 1, 2, \cdots$) are constant symmetric matrices that can be determined using a finite element analysis method. The scaling law for the lattice cellular structure can be formulated from the FEA simulation results as a function of the density. Based on Hashin–Shtrikman bounds the valid range of relative density is 0.41 to 0.76 for 2D lattice structures [29]. Similarly, the valid range of relative density is 0.44 to 0.79 for 3D lattice structures. Therefore, the lower actual cross-sectional area of the strut is obtained using Eqs. (8) and (9):

$$\rho_v = \frac{\rho^*}{\rho_s} = c_0 \frac{d_{\min}}{l}, \tag{8}$$

$$Ar_{\min} = \pi \left(\frac{d_{\min}}{2} \right)^2, \tag{9}$$

where c_0 is a near-unity numerical constant, $d_{\min}$ is the diameter of the strut, l is the length of the strut, and $Ar_{\min}$ is the lower value of the actual cross-sectional area. Therefore, the scaling factor Sf can be calculated to determine appropriate values for the cross-sectional areas of all the struts. The values of $\boldsymbol{Ar}$ are then scaled accordingly:

$$Sf = \frac{Ar_{\min}}{\min(\boldsymbol{Ar})}, \tag{10}$$

$$\boldsymbol{Ar} = Sf \cdot \boldsymbol{Ar}. \tag{11}$$

Using Eqs. (4)–(11), the lattice structures can be generated, and the structural strength of the obtained design can be guaranteed based on the equivalent elastic modulus of lattice structures. The overall process of the proposed LRDM method is summarized in Figure 3.

The main difference between RDM and LRDM is that the RDM process starts with two inputs: the information from the topology optimization and a coarse FEM, while the LRDM process starts with only one input: the topology optimization. Secondly, the key principles of RDM
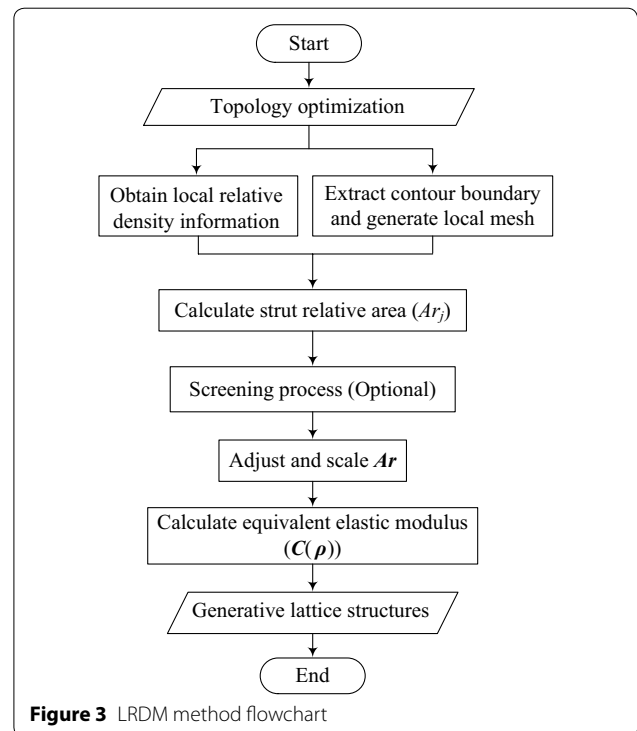

Figure 3 LRDM method flowchart

Song *et al. Chin. J. Mech. Eng.* (2018) 31:89

Page 5 of 9

Table 1 2D and 3D beams

Properties	Case 1	Case 2	Case 3	Case 4
Length (mm)	80	40	80	40
Height (mm)	20	10	40	10
Thickness (mm)	4	1	1	4
Loading magnitude (N)	100	1	1	1
Elasticity modulus (MPa)	1960	1960	1960	1960

and LRDM are essentially different. The RDM method depends on the relative densities of all the elements and all the FEMs in the design region, while the LRDM method only requires the relative densities of the local elements and local FEM. Thirdly, different formulas are used to calculate the strut relative area in each method. A weighted average is used in the RDM method while a geometric mean is used in the LRDM. Furthermore, the formulas used to calculate the scaling factor ***Ar*** and the vector min(***Ar***) are also different.

3.2 LRDM Method Validation

To validate the hypothesis of the LRDM method as well as to address the effect of the constant k and the distance r_{ij} on the weight function in Eq. (5), a simply supported beam is considered. The structure of the beam is similar to that in Ref. [29]. The design domain is discretized using 80×20 elements, the volume fraction is 0.35, and the properties of the beam are shown in Table 1 (case 1). A penalization factor of 3 is used in the optimization process in all cases in this paper. Two 2D lattice structures are generated in the RDM method and LRDM method using the relative density information obtained from by-products of the topology optimization. The same unit-cell type and unit-cell sizes are used in both the methods. The effects of different constant k and the distance r_{ij} on the weight function are shown in Figure 4a. As shown in the Figure, an increase in r_{ij} leads to a reduction in the weight function $\omega(r_{ij})$ until a zero value is reached for a given different constant k ($k = 0. 2, 0.3, 0.4, 0.6, 0.8,$ and 1.0). The trends in these curves show that the strut's relative cross-sectional area has no effect on the relative density elements that are beyond a certain distance from the strut his result is also shown in Figure 4b. It was found that an increase in the radius R leads to a reduction in the tip displacement until a final steady-state value is reached; however, the corresponding solution time has been substantially increased. Therefore, it is reasonable to rely on the contribution of local relative density elements.

In order to precisely test the solution time of the RDM and LRDM methods, the same unit-cell type is used to generate the 2D lattice structures. The second
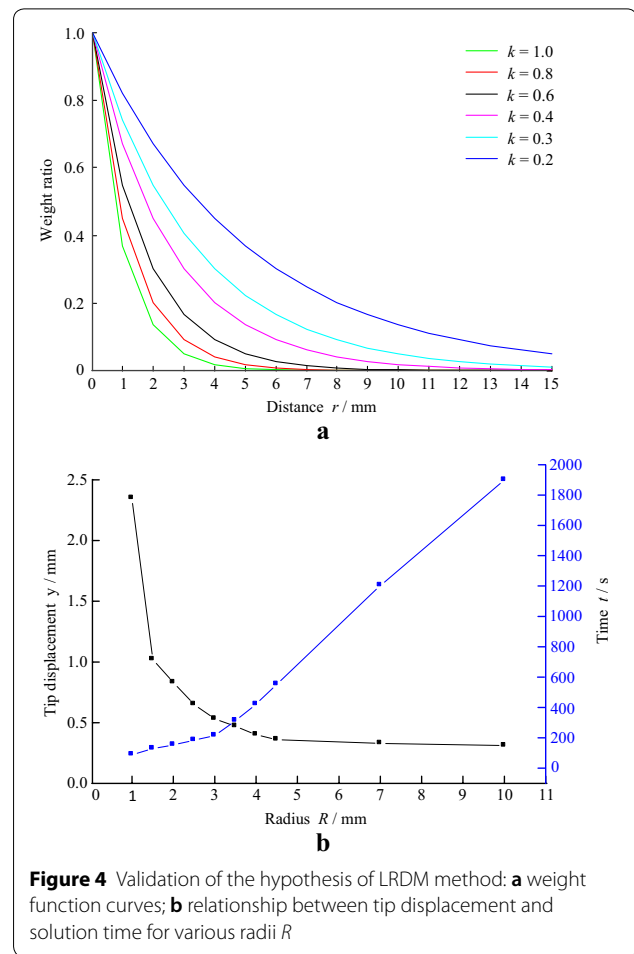

Figure 4 Validation of the hypothesis of LRDM method: **a** weight function curves; **b** relationship between tip displacement and solution time for various radii R

case (Table 1) is the same as that in Ref. [23], which is a cantilevered beam loaded at the middle of the right tip using the same topology optimization results. The lattice structures are generated using the RDM method with the lower relative cross-sectional value of 0.01, the size of the element is 2.5 mm×2.5 mm. While the LRDM method uses the same unit-cell type, R=6.5 mm and k=1.0.

The solution times for the RDM method are 30 s for generating the lattice structure and only 11 s for generating the lattice structure using the LRDM method. The RDM method requires more time to calculate the distance of all the relative density elements from each strut in the FEM. As for the LRDM method, it only calculates some of the relative density elements that are located in the range of a circle of radius 6.5 mm with its center at the midpoint of the strut. The RDM method produced the smallest tip displacement of 0.635 mm. The LRDM method result had a displacement of 0.613 mm, which is only 3.5% lower than that obtained with the RDM method. The results show that the LRDM method

Song *et al. Chin. J. Mech. Eng.*   (2018) 31:89

Page 6 of 9

is more efficient with respect to computational costs as compared with the RDM method for almost the same structural strength. Here, we note that our method cannot only be applied to the global FEM but is also suitable for the local FEM.

To test the computational accuracy and convergence of the RDM and LRDM methods, three elements of different sizes are generated using RDM and LRDM and the same topology optimization result. There are two types of unit-cells with a set size L of 1 mm×1 mm, 2 mm×2 mm, 3 mm×3 mm and 1 mm, 2 mm, and 3 mm, respectively. A regular triangular unit-cell is chosen for the comparison between the RDM and LRDM methods because it is convenient for controlling the unit-cell size. A 2D cantilever beam is used, and the design domain is discretized into 80×20 elements. Figure 5 shows the lattice structure generated using the RDM and LRDM methods for $R = 3L$. The results of the computation accuracy and convergence of the RDM and LRDM methods are summarized in Table 2.

Table 2 shows that the average computation accuracy of RDM is 2.05% higher than that of LRDM. One possible reason is that the total volume of the generated lattice structure must meet the volume constraint in the RDM method. The average iterative number for RDM is 43.62% higher than that for LRDM. The main reason for this is the use of the local relative density information and the triangular mesh.

4 Case Illustrations and Analysis

4.1 2D Cantilever Beam

To demonstrate the performance of the LRDM method, a 2D cantilever beam is used with the SIMP method. The third case is similar to that in Ref. [30]. The design domain is discretized into 80×40 elements, and a vertical unit force is considered at the middle of the right end of

Table 2 Test results of computation accuracy and convergence for RDM and LRDM methods

Method	Mesh size (mm)	Target volume (mm³)	Optimized volume (mm³)	Iteration no.
RDM	1 × 1	50	48.1304	143
LRDM	1	50	47.7206	84
RDM	2 × 2	40	38.0690	86
LRDM	2	40	37.0607	51
RDM	3 × 3	30	27.8695	45
LRDM	3	30	27.0312	23

the beam. The properties of the 2D cantilever beam are shown in Table 1 (case 3). Figure 6a, b show the results of the topology optimization and the generation of the FEM with the same unit-cell size of 1 mm. The lower relative cross-sectional area and the rejection ratio are set as 0.001 and 0.1, respectively for the RDM method. As for the LRDM method, the radius is 6.5 times the length of the cell of the density element. Figure 6c, d show the generated lattice structure with 616 and 587 struts using the RDM and LRDM methods respectively. The RDM method result showed the smallest tip displacement of 0.383 mm. The LRDM method result showed a displacement of 0.347 mm, which was 9.4% lower than that obtained with the RDM method. The solution time for generating the lattice structure with the RDM method was 76 s and only 32 s in the case of the LRDM method.

The reason why different proportions for case 2 and case 3 is that the same FEM is used to map the topology optimization result to the lattice structure with RDM and LRDM methods respectively in case 2. The various FEMs are adopted to generate different lattice structures with RDM and LRDM in case 3. Thus, the various FEMs may
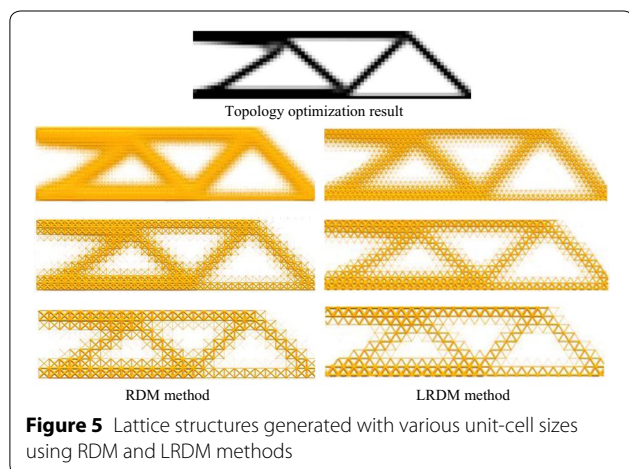

Figure 5 Lattice structures generated with various unit-cell sizes using RDM and LRDM methods
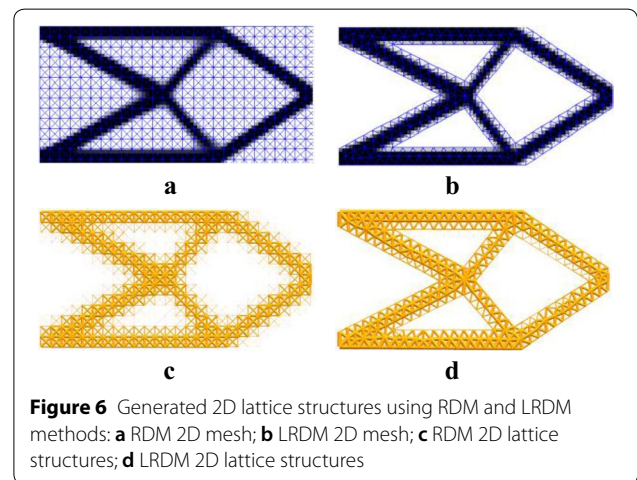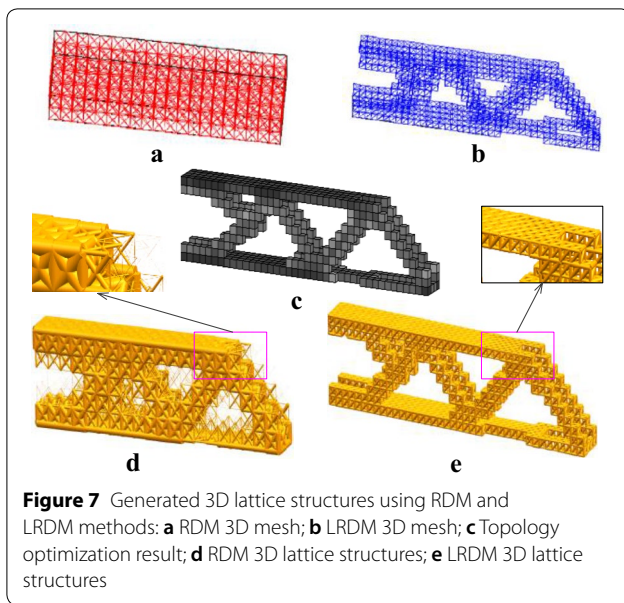

Figure 6 Generated 2D lattice structures using RDM and LRDM methods: **a** RDM 2D mesh; **b** LRDM 2D mesh; **c** RDM 2D lattice structures; **d** LRDM 2D lattice structures

Song *et al. Chin. J. Mech. Eng.*   (2018) 31:89

Page 7 of 9

Figure 7 Generated 3D lattice structures using RDM and LRDM methods: **a** RDM 3D mesh; **b** LRDM 3D mesh; **c** Topology optimization result; **d** RDM 3D lattice structures; **e** LRDM 3D lattice structures

Figure 8 Comparison of tip displacement of generated lattice structure for various volume fractions

result in different proportions of the LRDM method to some extent.

4.2 3D Cantilever Beam

To verify the effectiveness of the proposed method, a 3D cantilever beam is used to generate a lattice structure using the LRDM method, which is then compared with that obtained using the RDM method. The beam has a length of 40 mm, height of 10 mm, and thickness of 4 mm. The properties of the 3D cantilever beam are shown in Table 1 (case 4). The prismatic design is fully constrained at one end and a unit distributed vertical load is applied downwards on the lower free edge. Figure 7a shows the topology optimization result for solving the minimum compliance problem under a 30% volume fraction constraint. Figure 7b shows the generated FEM with a unit-cell size of 2 mm × 2 mm, and the unit-cell type is the same as that used with the RDM method. Figure 7c shows the FEM generated using the Delaunay algorithm with a unit-cell size of 1 mm × 1 mm. Figure 7d, e show the 3D lattice structures generated using the RDM and LRDM methods, respectively, with the same volume constraint.

The variation in the tip displacement and solution time of the generated lattice structures are displayed in Figures 8 and 9 for various volume fractions. An increase in the volume fraction leads to a reduction in the tip displacement while the displacement gap of the RDM and LRDM methods is also gradually reduced. The gap reduction in the tip displacement is caused by the gradual removal of the partial volume in the topology optimization process.
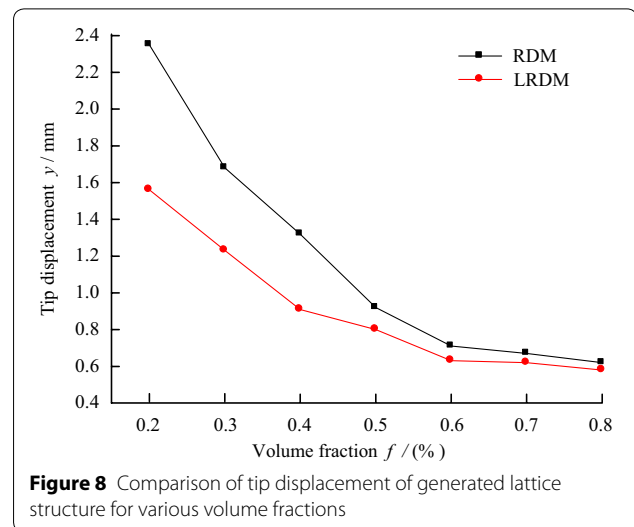
It should be noted that the solution time for the lattice structure generated using the RDM method remains almost unchanged as the volume fraction of the topology optimization increases. In the case of the LRDM method, the solution time of the generated lattice structure increases gradually as the volume fraction increases in the topology optimization, but the solution time is still less than that of the RDM method. The reason for this phenomenon is that the computational cost is relate to the number of FEMs and relative density elements. In the case of the RDM method, the number of FEMs is fixed once the initial design area is set; however, the number of FEMs increases with the increase in the volume fraction of the LRDM method during the mapping process.

In order to test the structural strength of the lattice structures using the two models from Figure 7d, e, we print them with the help of a MakerBot Replicator 2 printer using fused deposition modeling technology. We use a plastic PC-ABS material with a yield strength of 4.1×10^7 N/m². An electromechanical universal testing machine (HUALONG WDW-100) is used to evaluate the strength of the printed lattice structures. We ran compression tests for the two printed lattice structures. The 2460.467 g lattice structure that was tested using the RDM method could resist a force of 983.7 N; the other lattice structure tested using the LRDM method, failed at an applied force of 1153.5 N with a mass of 2450.074 g. Therefore, the calculated strength-to-weight ratio of the LRDM method is 14.83% higher than that of the RDM method. Moreover, we can calculate the strength using a simple formula based on the volumetric density [23]. The volume fraction of the lattice structures optimized with the RDM and LRDM are 0.3045% and 0.3568%, respectively. The theoretical calculation results are 14.65%

Song *et al. Chin. J. Mech. Eng.* (2018) 31:89

Page 8 of 9

Figure 9 Comparison of the solution time of generated lattice structure for various volume fractions

Figure 10 Generated procedure of jet engine bracket with lattice structures
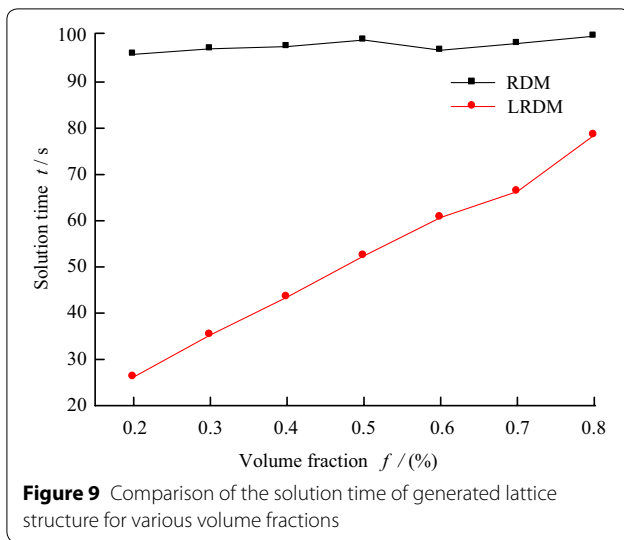
higher than that obtained with the RDM, which almost the same as the experiment results.

4.3 Micro Jet Engine Bracket

To demonstrate the applicability of the LRDM method for complex 3D structures, a micro jet engine bracket [31] is designed and optimized using a continuum topology optimization (SIMP). The optimization problem can be stated as follows:

$$
\min c(\boldsymbol{x}) = \boldsymbol{U}^\mathrm{T} \boldsymbol{K} \boldsymbol{U} = \sum_{e=1}^{N} E_e(x_e) \boldsymbol{u}_e^\mathrm{T} \boldsymbol{k}_0 \boldsymbol{u}_e,
$$
$$
\text{s.t., } V(\boldsymbol{x})/V_0 = f, \tag{12}
$$
$$
\boldsymbol{K}\boldsymbol{U} = \boldsymbol{F},
$$
$$
0 \le \boldsymbol{x} \le 1,
$$

where c is the compliance, $\boldsymbol{U}$ and $\boldsymbol{F}$ are the global force vector and displacement respectively; $\boldsymbol{K}$ is the global stiffness matrix, x_e is the element density, $V(\boldsymbol{x})$ is the lattice structure volume, V_0 is the design domain volume, and f is the prescribed volume fraction. Here, $V_0 = 480000$ mm^3, $f=0.3$, and $F=42000$ N. The bracket is to be subjected to two loads and supported as shown in Figure 10b. Figure 10a shows the original bracket model. Figure 10c shows an optimized 3D model obtained using the topology optimization. Figure 10d shows the lattice structures with 5837 struts that are generated using the LRDM method. The solution time for the LRDM method is 2468 s. The RDM method would not be able to generate a complex mesh, as the RDM would not be a feasible choice in this case. As compared to the topology optimization, it can be estimated that LRDM saves 9.8% material despite its longer generation time.
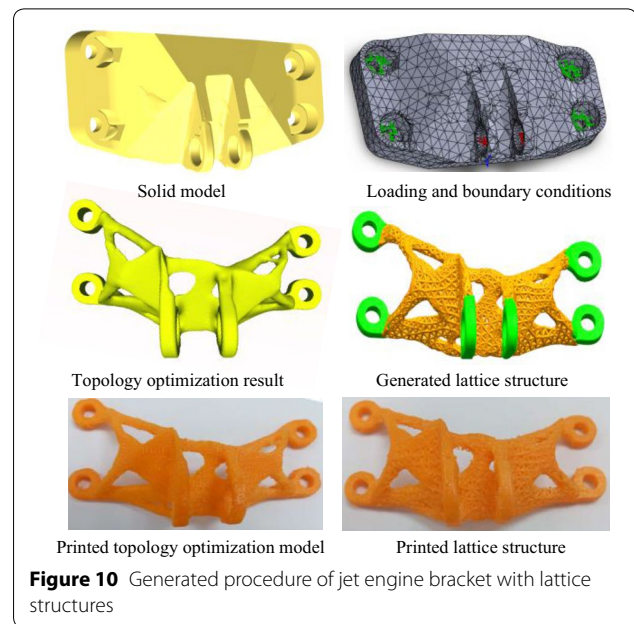
5 Conclusions

1. The average iterative number of RDM is 43.62% higher than that of LRDM, and the average computation accuracy of RDM is 2.05% higher than that of LRDM for the same two-dimensional mesh.
2. As compared to the continuum topology optimization, the LRDM method can save approximately 9.8% 3D printing material for the same 3D model.
3. It is no contributions to the strut's relative cross-sectional diameter to the relative density elements that are beyond a certain distance away from the strut for RDM and LRDM method.
4. The solution time of the lattice structures generated using the LRDM method is approximately 50% lower than that of the RDM method.

Authors' Contributions
G-HS and S-KJ was in charge of the whole trial; F-LZ and Y-DW wrote the manuscript; HX and L-FQ assisted with sampling and laboratory analyses. All authors read and approved the final manuscript.

Author Details
[1] Beijing Xinghang Mechanical-electrical Equipment Co. Ltd., Beijing 100074, China. [2] School of Mechanical Engineering, Beijing Institute of Technology, Beijing 100081, China.

Song *et al. Chin. J. Mech. Eng.*   (2018) 31:89

Page 9 of 9

knowledge management, design theory and method, and manufacturing services technology.

Fang-Lei Zhao, born in 1991, is currently a master candidate at *School of Mechanical Engineering, Beijing Institute of Technology, China*. His main research interests include additive manufacturing and functionally graded materials.

Ye-Dong Wang, born in 1993, is currently a master candidate at *School of Mechanical Engineering, Beijing Institute of Technology, China*. His main research interests include additive manufacturing and functionally graded materials.

Hao Xing, born in 1991, is currently a master candidate at *School of Mechanical Engineering, Beijing Institute of Technology, China*. His main research interests include additive manufacturing and functionally graded materials.

Long-Fei Qie, born in 1989, is currently a PhD candidate at *School of Mechanical Engineering, Beijing Institute of Technology, China*. His main research interests include additive manufacturing and topology optimization.

Competing Interests
The authors declare that they have no competing interests.

Publisher's Note
Springer Nature remains neutral with regard to jurisdictional claims in published maps and institutional affiliations.

References
[1] Gibson, D W Rosen, B Stucker. *Additive manufacturing technologies*. New York: Springer, 2010: 283–300.
[2] J Banhart. Manufacture, characterisation and application of cellular metals and metal foams. *Progress in Materials Science*, 2001, 46(6): 559–632.
[3] A G Evans, J W Hutchinson, N A Fleck, et al. The topological design of multifunctional cellular metals. *Progress in Materials Science*, 2001, 46(3): 309–327.
[4] A Takezawa, M Kobashi, M Kitamura. Porous composite with negative thermal expansion obtained by photopolymer additive manufacturing. *APL Materials*, 2015, 3(7): 076103.
[5] L J Gibson. Biomechanics of cellular solids. *Journal of Biomechanics*, 2005, 38(3): 377–399.
[6] S Varanasi, J S Bolton, T H Siegmund, et al. The low frequency performance of metamaterial barriers based on cellular structures. *Applied Acoustics*, 2013, 74(4): 485–495.
[7] H V Wang, D W Rosen. *Computer-aided design methods for the additive fabrication of truss structure*. School of Mechanical Engineering, Georgia Institute of Technology, 2001.
[8] J C Wallach, L J Gibson. Mechanical behavior of a three-dimensional truss material. *International Journal of Solids and Structures*, 2001, 38(40): 7181–7196.
[9] H Wang, D W Rosen. Parametric modeling method for truss structures. *ASME 2002 International Design Engineering Technical Conferences and Computers and Information in Engineering Conference*, Quebec, Canada, September 29–October 2, 2002: 759–767.
[10] H V Wang. *A unit cell approach for lightweight structure and compliant mechanism*. Georgia Institute of Technology, 2005.
[11] H Wang, Y Chen, D W Rosen. A hybrid geometric modeling method for large scale conformal cellular structures. *ASME 2005 International Design Engineering Technical Conferences and Computers and Information in Engineering Conference*, Long Beach, USA, September 24–28, 2005: 421–427.
[12] S Gonella, M Ruzzene. Homogenization and equivalent in-plane properties of two-dimensional periodic lattices. *International Journal of Solids and Structures*, 2008, 45(10): 2897–2915.
[13] J Patel, S K Choi. Classification approach for reliability-based topology optimization using probabilistic neural networks. *Structural and Multidisciplinary Optimization*, 2012, 45(4): 529–543.
[14] J Chu, S Engelbrecht, G Graf, et al. A comparison of synthesis methods for cellular structures with application to additive manufacturing. *Rapid Prototyping Journal*, 2010, 16(4): 275–283.
[15] L Liu, J Yan, G Cheng. Optimum structure with homogeneous optimum truss-like material. *Computers & Structures*, 2008, 86(13): 1417–1425.
[16] D Rosen. Design for additive manufacturing: past, present, and future directions. *Journal of Mechanical Design*, 2014, 136(9): 090301.
[17] Y Tang, A Kurtz, Y F Zhao. Bidirectional evolutionary structural optimization (BESO) based design method for lattice structure to be fabricated by additive manufacturing. *Computer-Aided Design*, 2015, 69: 91–101.
[18] T Stankovic, J Mueller, P Egan, et al. A generalized optimality criteria method for optimization of additively manufactured multimaterial lattice structures. *Journal of Mechanical Design*, 2015, 137(11): 111405.
[19] G C Graf, J Chu, S Engelbrecht, et al. Synthesis methods for lightweight lattice structures. *ASME 2009 International Design Engineering Technical Conferences and Computers and Information in Engineering Conference*, San Diego, California, USA, January 01, 2009: 579–589.
[20] P S Chang, D W Rosen. An improved size, matching, and scaling method for the design of deterministic mesoscale truss structures. *ASME 2011 International Design Engineering Technical Conferences and Computers and Information in Engineering Conference*, Washington DC, USA, 2011: 697–707.
[21] P S Chang, D W Rosen. The size matching and scaling method: a synthesis method for the design of mesoscale cellular structures. *International Journal of Computer Integrated Manufacturing*, 2013, 26(10): 907–927.
[22] J Nguyen, S Park, D W Rosen. Heuristic optimization method for cellular structure design of light weight components. *International Journal of Precision Engineering and Manufacturing*, 2013, 14(6): 1071–1078.
[23] M Alzahrani, S K Choi, D W Rosen. Design of truss-like cellular structures using relative density mapping method. *Materials & Design*, 2015, 85: 349–360.
[24] A V Kumar, D C Gossard. Synthesis of optimal shape and topology of structures. *Journal of Mechanical Design*, 1996, 118(1): 68–74.
[25] M Bern, D Eppstein. Mesh generation and optimal triangulation. *Computing in Euclidean Geometry*, 1995, 4: 47–123.
[26] S H Lo. A new mesh generation scheme for arbitrary planar domains. *International Journal for Numerical Methods in Engineering*, 1985, 21(8): 1403–1426.
[27] P O Persson, G Strang. A simple mesh generator in MATLAB. *SIAM Review*, 2004, 46(2): 329–345.
[28] L J Gibson, M F Ashby. *Cellular solids: structure and properties*. Cambridge University Press, 1999.
[29] P Zhang, J Toman, Y Yu, et al. Efficient design-optimization of variable-density hexagonal cellular structure by additive manufacturing: theory and validation. *Journal of Manufacturing Science and Engineering*, 2015, 137(2): 021004.
[30] E Biyili, A C To. Proportional topology optimization: a new non-gradient method for solving stress constrained and minimum compliance problems and its implementation in MATLAB. *Plos One*, 2015, 10(12): e0145041.
[31] H D Morgan, H U Levatti, J Sienz, et al. GE Jet engine bracket challenge: a case study in sustainable design. *Sustainable Design and Manufacturing 2014 Part 1*, 2014: 95–107.